Tunable Resins with PDMS-like Elastic Modulus for Stereolithographic 3D-printing of Multimaterial Microfluidic Actuators

Alireza Ahmadianyazdi*,1, Isaac J. Miller[2], and Albert Folch[1]

*1*Department of Bioengineering, University of Washington, Seattle, WA, 98105

*2*Department of Chemical Engineering, University of Washington, Seattle, WA, 98105
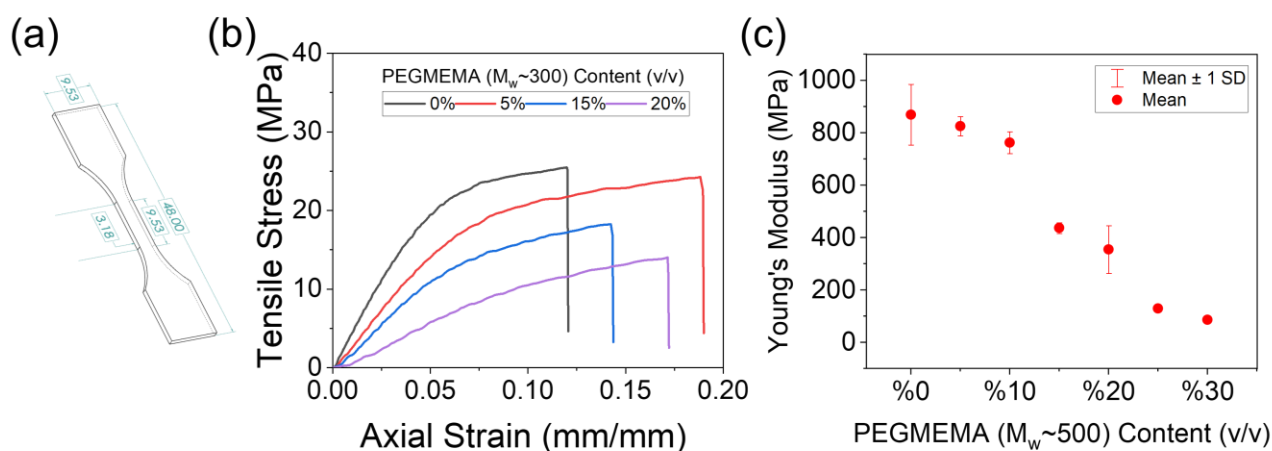
Corresponding author, e-mail address: aahmad33@uw.edu

Fig. S1. Mechanical behavior of PEGDA-*co*-PEGMEMA plastics. (a) 3D schematic of the dog-bone specimen 3D-printed to measure the elastic properties of the PEGDA-*co*-PEGMEMA plastics. The dimensions are in mm. (b) Representative stress-strain curves for PEGDA-*co*-PEGMEMA plastics with PEGMEMA monomers at M_w~300. (c) Young's modulus of PEGDA-*co*-PEGMEMA derived plastics (PEGDA at M_w ~ 258, and PEGMEMA at M_w ~ 500).

To obtain the Young's modulus of 40% PEGDA-*co*-PEGMEMA plastics, we employed the analysis of membrane deflection presented in ref.[1] (similarly in refs. [2,3]). In this analysis, the following equation is fitted to the pressure (P) versus deflection (h) measurements of a circular membrane:

$$P = Ah + \frac{8Et}{3a^4(1-v)}h^3 \qquad (S1)$$

where E is the Young's modulus, v is the Poisson' ratio, a denotes the membrane radius, t is the membrane thickness, and A accounts for the initial stress or slack in the membrane. Eq. S1 is

then fitted to the pressure-displacement data of 40% PEGDA-*co*-PEGMEMA membrane in Fig. S2. Assuming a Poisson's ratio of 0.35 used to evaluate poly(methyl methacrylate) plastics,[4,5] E is obtained as ~2.24 MPa.
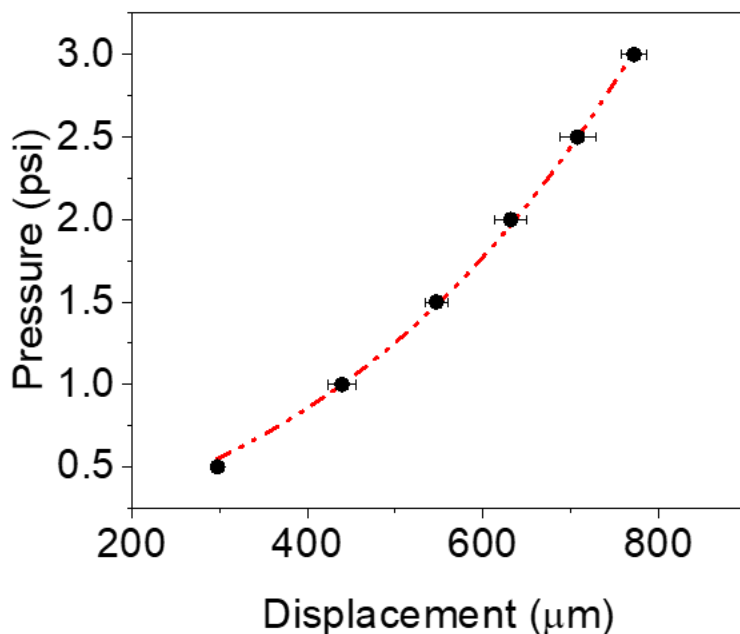

Fig. S2. Pressure-displacement data for a 40% PEGDA-*co*-PEGMEMA membrane. The dashed line represents the fitted curve according to Eq. S1. The membrane has a thickness t of ~60 μm and a radius a of 1 mm.
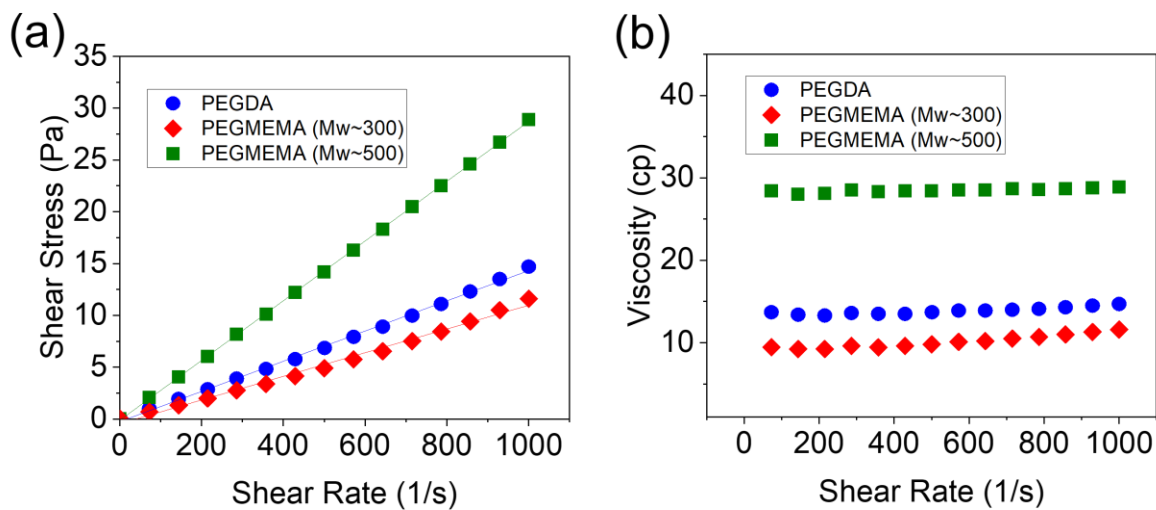

Fig. S3. Rheological behavior of PEGDA and PEGMEMA monomers. Plots of (a) shear stress and (b) viscosity with respect to shear rate for PEGDA and PEGMEMA (M_w~300 and 500) monomers.

The data in (a) are fitted with a straight line (R^2_{avg}~0.98), confirming Newtonian rheology for the given range of applied shear rates. From the graphs in (b), the average viscosities are obtained as ~13.86 cp for PEGDA, ~10.88 cp for PEGMEMA with M_w~300, and ~28.50 for PEGMEMA with M_w~500.
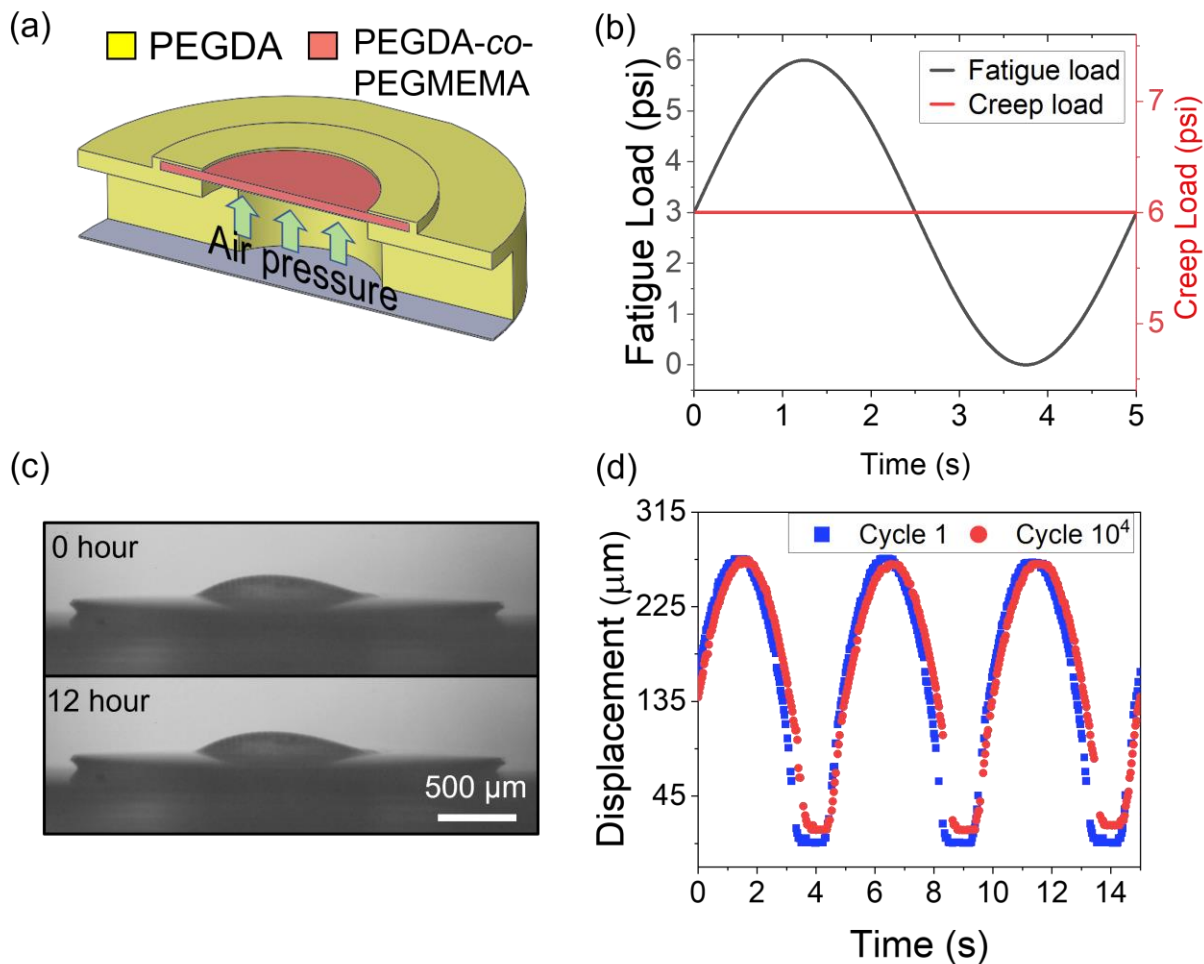

Fig. S4. Creep and fatigue of PEGDA-*co*-PEGMEMA plastics. (a) Cut-away view of the 3D model of the membrane testing device used to investigate elastic behavior of PEGDD-*co*-PEGMEMA membranes. (b) Creep and fatigue loading signals for evaluating the membrane tolerance. (c) Microscope image of the deflected membrane before and after 12 hours of applied creep load. (d) Comparison of the membrane displacement before and after 10^4 cyclic loading shown in (b), suggesting minimal membrane fatigue (less than *ca.* 4.5% difference between the two recorded displacement curves). The displacement data were obtained by recording the video of membrane movement, and tracking its peak height (in the middle of the membrane) with an open-source video tracking software.
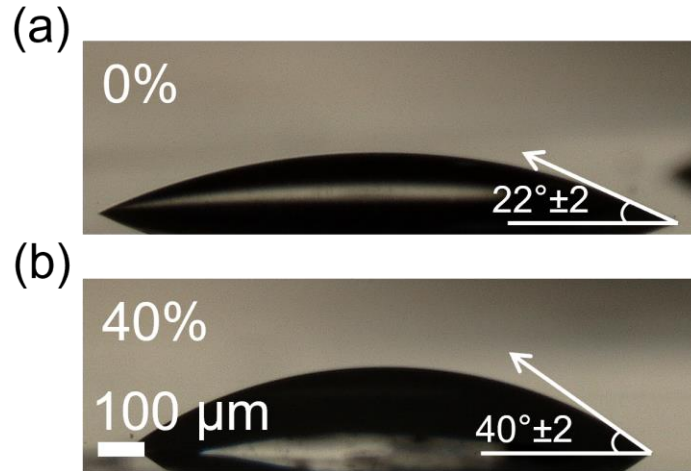
Fig. S5. **Contact angle measurements.** (a) Contact angle of a 5 µL droplet of water on a 3D-printed surface of (a) 0, and (b) 40% PEGDA-*co*-PEGMEMA surface.
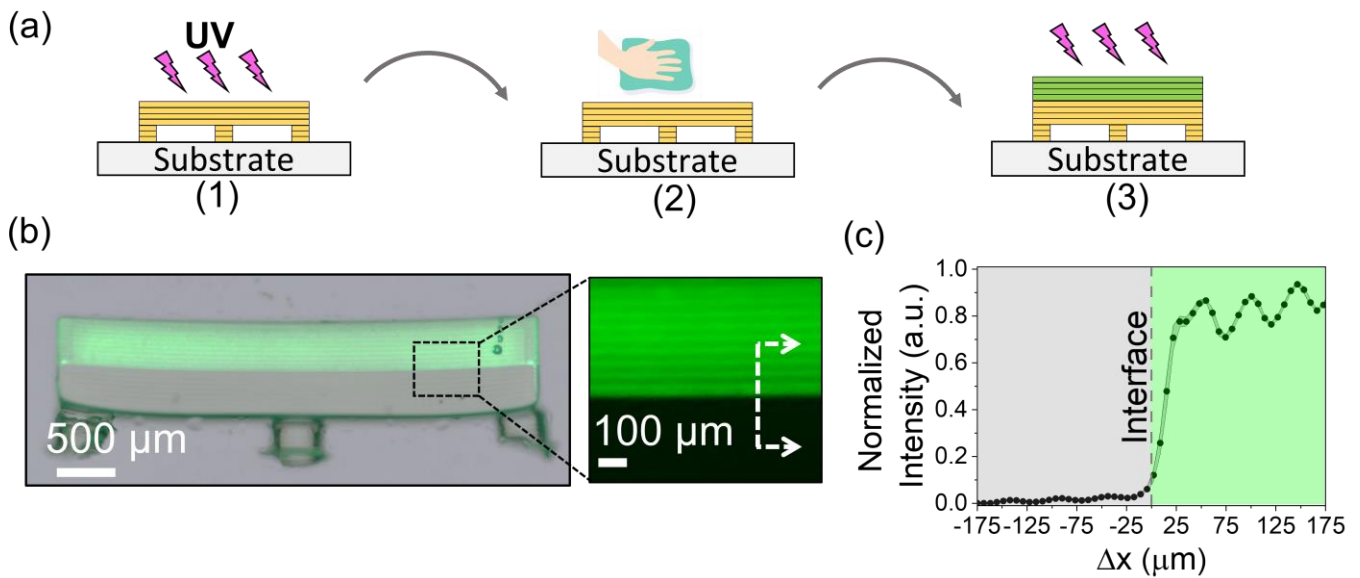

Fig. S6. **Print-pause-print method.** (a) Cross-section schematic of the print-pause-print (PPP) protocol. (b) Fluorescent overlay micrograph of a 3P-printed multimaterial print. Here we used two resins: plain PEGDA and a mixture of PEGDA and sodium fluorescein salt that fluoresces green. The close-up image is the fluorescent image of the interface between the two resins. (c) Fluorescent intensity across the interface shown by the dashed line in image (b).

At any dosage of UV light energy, the cured depth d_c of the resin is related to the exposure time t_c *via* the following equation:[6]

$$d_c = d_0 \ln \left(\frac{t_c}{t_0} \right) \tag{S2}$$

where d_0 is the characteristic curing depth (maximum depth of resin that can be cured by a given UV light energy) and t_0 is the characteristic curing time (critical exposure time needed to initiate polymerization). d_0 and t_0 can be obtained for any resin and SLA printer from experimental measurements of d_c with respect to t_c. Therefore, d_0 and t_0 are parameters that can be used to predict the curing behavior of the resin such that, at a given d_0, lower t_0 correlates with higher resin reactivity.[7] Eq. S2 was fitted to the cured depth measurements of 0, 20, and 40% PEGDA-*co*-PEGMEMA resins in Fig. S5. Table S1 shows the calculated values for d_0 and t_0 for each resin, demonstrating an average t_0 of ~1 s. Note that the ultimate printing resolution of the PEGDA-*co*-PEGMEMA is dictated by the XYZ resolution of the 3D-printer and the concentration of photo-absorber (ITX) and initiator (Irgacure-819), as studied by many groups[8–11], including ours[12–16] extensively.
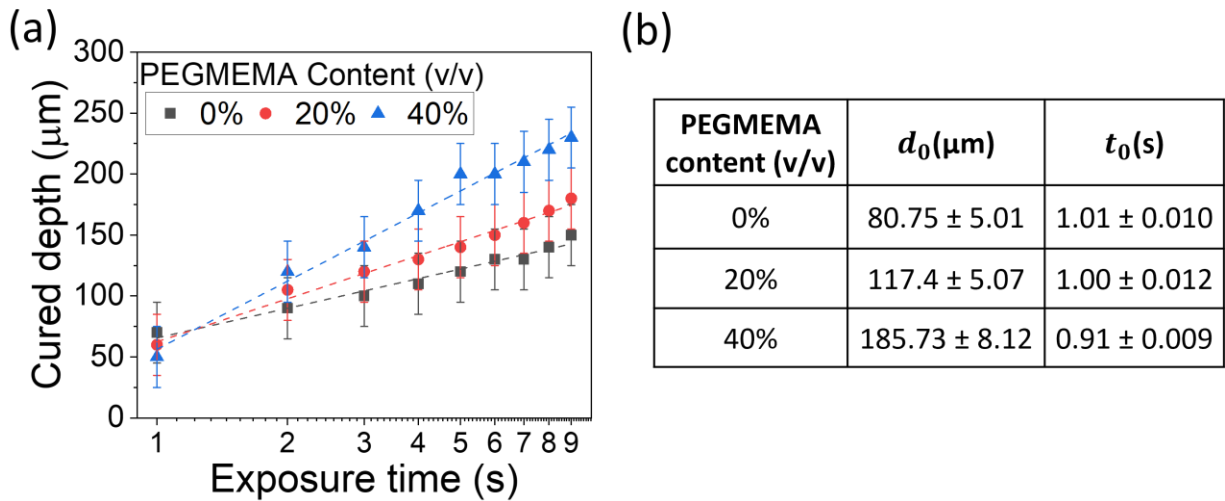

(a)

(b)

PEGMEMA content (v/v)	d_0(μm)	t_0(s)
0%	80.75 ± 5.01	1.01 ± 0.010
20%	117.4 ± 5.07	1.00 ± 0.012
40%	185.73 ± 8.12	0.91 ± 0.009

Fig. S7. PEGDA-*co*-PEGMEMA curing behavior. (a) Cured depth d_c versus exposure time t_c for the PEGDA-*co*-PEGMEMA resin containing varying amounts of PEGMEMA monomers. (b) Characteristic curing depth d_0 and curing time t_0 of PEGDA-*co*-PEGMEMA resins.
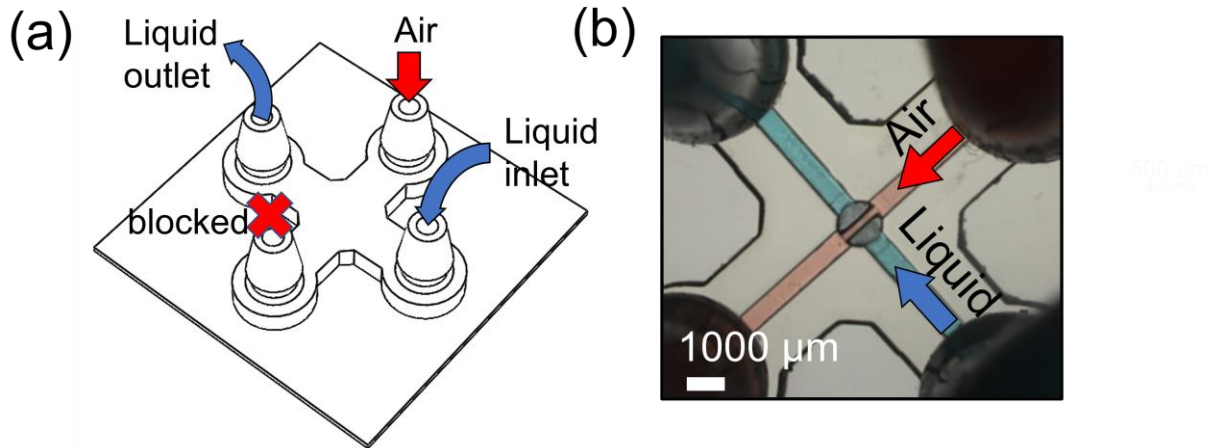
Fig. S8. Experimental setup for the evaluation of microvalves. (a) 3D schematic of the air and liquid connections to test the microvalve performance. (b) Micrograph of the 3P-printed microvalve with air and liquid channels dyed with colors for visual clarity. The valve is in an open state.
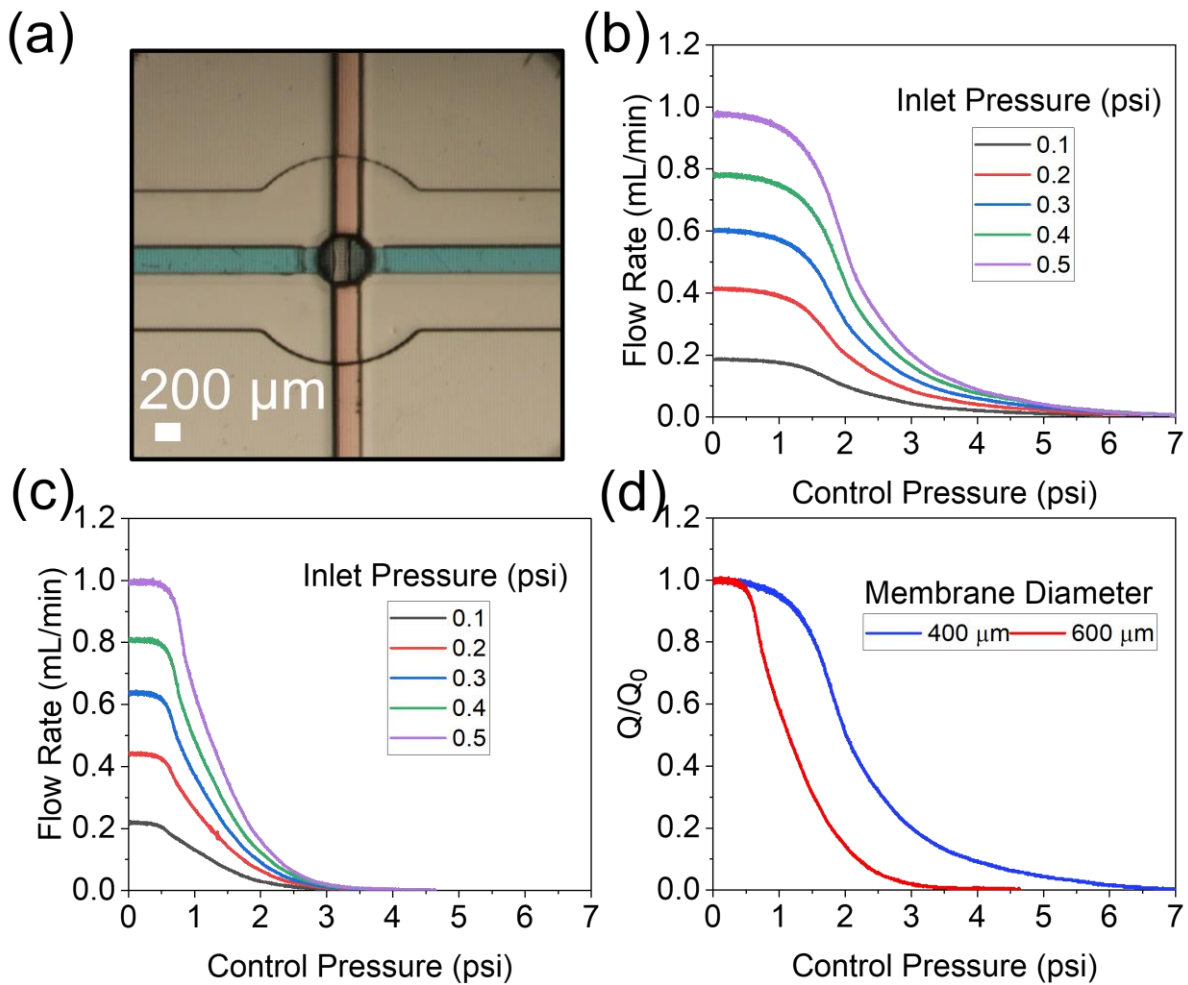
Fig. S9. High-resolution PEGDA-*co*-PEGMEMA microvalves. (a) Micrograph of a 3P-printed microvalve with membrane of diameter 400 μm made from 40% PEGDA-*co*-PEGMEMA. The valve is in an open state. The microchannels are 200 μm wide and 200 μm deep. Flow rate versus control pressure for microvalves 3P-printed with 40% PEGDA-*co*-PEGMEMA membrane that has a diameter of (b) 400 μm and (c) 600 μm. (d) Normalized flow rate Q/Q_0 versus control pressure for microvalves in (b) and (c) at 0.3 psi of inlet flow pressure. Note that the thickness of the membranes in all microvalves is kept at 50 ± 10 μm and the valve seat has a width of 100 μm. The STL files for these high-resolution microvalves are available in the Supplementary Information.
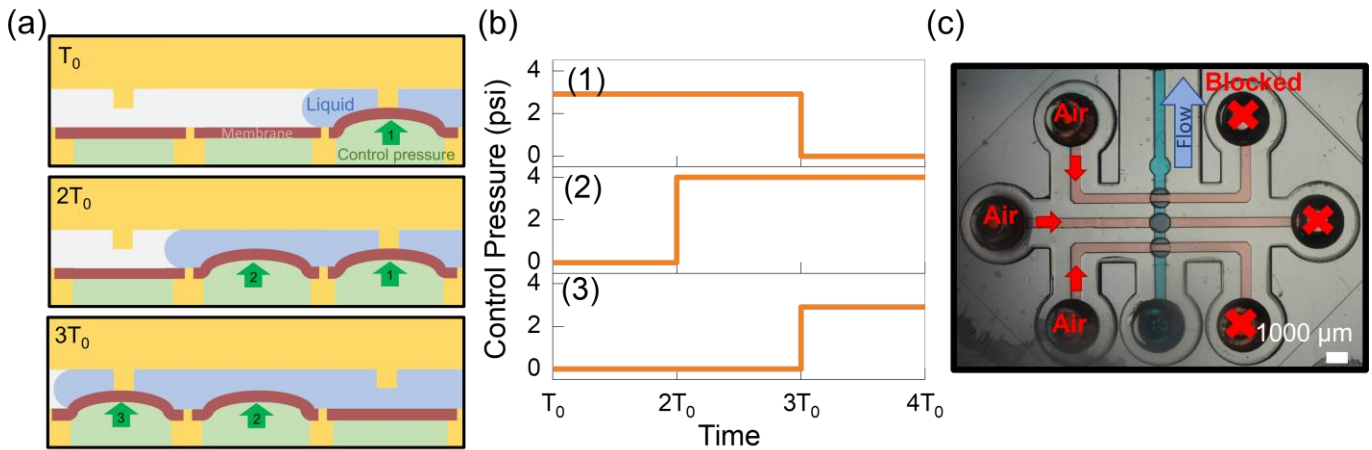

Fig. S10. Micropump operation and evaluation setup. (a) Cross-section schematic of the sequence of membrane deflections used to generate peristalsis. (b) Input pressure signals to each membrane of the micropump. (c) Micrograph of the 3P-printed micropump. To visualize the channels, the fluid channel carrying flow (blue arrow) was filled with blue food-coloring dye and the pneumatic channels were filled with red food-coloring dye; for pressurization (red arrows), the pneumatic outlets were blocked as indicated with red crosses. The valves are in an open state.
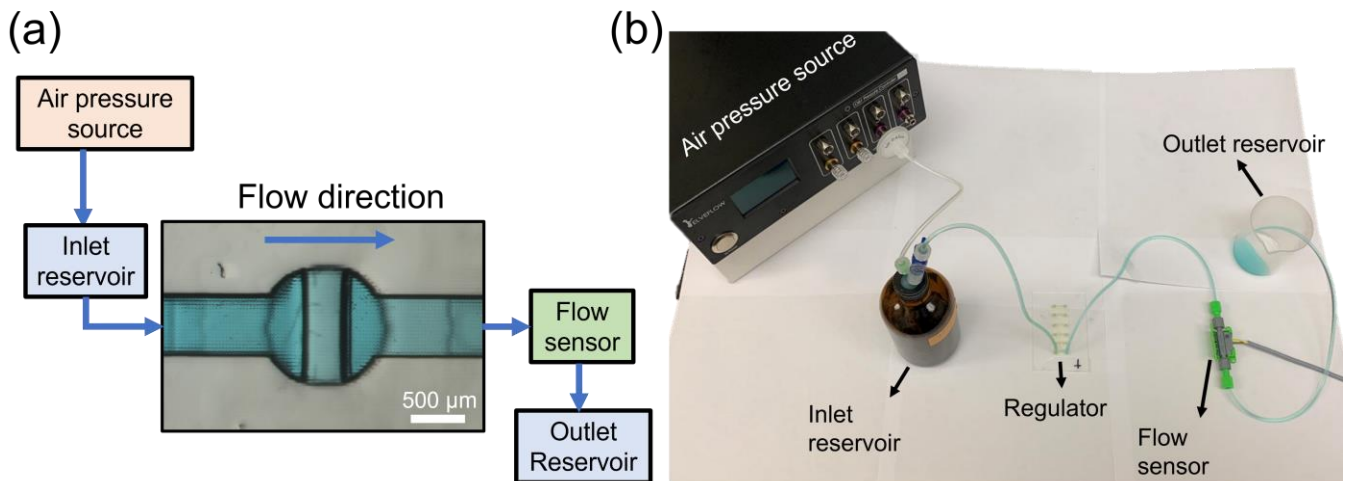
Fig. S11. Experimental setup for the 3P-printed flow regulator. (a) Schematic illustration and (b) photo of the setup used to test the performance of the 3P-printed regulator. The liquid water through the regulator is dyed with blue color (see Experimental section) for visualization.

References

[1]   M. K. Small, W. D. Nix, *J Mater Res* **1992**, *7*, 1553.

[2]   J. J. Vlassak, W. D. Nix, *J Mater Res* **1992**, *7*, 3242.

[3]   R. L. Edwards, G. Coles, W. N. Sharpe, *Exp Mech* **2004**, *44*, 49.

[4]   C. I. Rogers, J. B. Oxborrow, R. R. Anderson, L. F. Tsai, G. P. Nordin, A. T. Woolley, *Sens Actuators B Chem* **2014**, *191*, DOI 10.1016/j.snb.2013.10.008.

[5]   A. Goswami, A. M. Umarji, G. Madras, *Polym Adv Technol* **2012**, *23*, 1604.

[6]   N. Bhattacharjee, C. Parra-Cabrera, Y. T. Kim, A. P. Kuo, A. Folch, *Advanced materials* **2018**, *30*, 1800001.

[7]   G. Taormina, C. Sciancalepore, M. Messori, F. Bondioli, *J Appl Biomater Funct Mater* **2018**, *16*, 151.

[8]   H. Gong, A. T. Woolley, G. P. Nordin, *Lab Chip* **2018**, *18*, 639.

[9]   H. Gong, A. T. Woolley, G. P. Nordin, *Lab Chip* **2016**, *16*, 2450.

[10]   M. J. Beauchamp, G. P. Nordin, A. T. Woolley, *Anal Bioanal Chem* **2017**, *409*, 4311.

[11]   H. Gong, B. P. Bickham, A. T. Woolley, G. P. Nordin, *Lab Chip* **2017**, *17*, 2899.

[12]   A. Naderi, N. Bhattacharjee, A. Folch, *Annu Rev Biomed Eng* **2019**, *21*, 325.

[13]   A. K. Au, W. Huynh, L. F. Horowitz, A. Folch, *Angewandte Chemie International Edition* **2016**, *55*, 3862.

[14]   A. K. Au, H. Lai, B. R. Utela, A. Folch, *Micromachines (Basel)* **2011**, *2*, 179.

[15]   A. P. Kuo, N. Bhattacharjee, Y. S. Lee, K. Castro, Y. T. Kim, A. Folch, *Adv Mater Technol* **2019**, *4*, DOI 10.1002/admt.201800395.

[16]   A. Urrios, C. Parra-Cabrera, N. Bhattacharjee, A. M. Gonzalez-Suarez, L. G. Rigat-Brugarolas, U. Nallapatti, J. Samitier, C. A. DeForest, F. Posas, J. L. Garcia-Cordero, A. Folch, *Lab Chip* **2016**, *16*, 2287.